Numerical study of an airfoil interacting with the vortical wake of an upstream cylinder

Raj Solanki

National Institute of Technology Karnataka, Surathkal

Abstract

The current investigation focuses on the numerical analysis of the two-dimensional, unsteady, NACA0012 airfoil and circular cylinder interaction. This airfoil is placed at zero and five degrees angle of attack. OpenFOAM was used to perform simulations for the unsteady incompressible flow for turbulent conditions at a specified inlet velocity. For this study, three streamwise distances were considered: 2D, 6D, and 10D. In these expressions, D stands for the diameter of the circular cylinder, which is 25 mm. Direct comparison of flow fields shows pronounced wake-body interaction for small spacing, characterized by vortex generation with lift and drag fluctuations over the airfoil. Increasing the spacing causes changes in the wake and, thus, alters the flow along the path. Analysis of instantaneous and time-averaged velocity profiles, along with turbulence intensity contours, provides insight into the downstream movement of the wake and the fluid dynamics within each spacetime region. Notably, upstream wakes significantly affect downstream surfaces. This research quantifies the variation in unsteady forces as the distance between interacting surfaces changes. The simulations were performed over a finite period.

1. Introduction

The interaction between the wake of a bluff body and a downstream another body represents a critical phenomenon in many engineering applications, including aircraft in formation flight, wind-turbine arrays, and the arrangement of unmanned aerial vehicles. The separated flow reattaches as a Karman vortex street, which is characterized by periodic vortex shedding, when a circular cylinder is positioned in a uniform free-stream. In contrast to undisturbed conditions, the lift, drag, and overall flow field of any shaped body positioned

downstream are altered by the alternating fluid flow because of this formation of vortices formed because of the cylinder.

The spatial separation between the lifting surface and the bluff body must be systematically investigated in order to fully comprehend wake–airfoil interactions. Previous research has shown that while greater separations permit partial wake dissipation and more stable loading on the downstream body, close proximity (on the order of a few cylinder diameters) can cause significant fluctuations in aerodynamic coefficients. For laminar flows at moderate Reynolds numbers, the exact relation between spacing and unsteady force magnitudes—and the corresponding flow structures—remains uncharacterized.

The impact of cylinder wake on a NACA 0012 airfoil at zero and five degrees angle of attack is investigated in this work using two-dimensional, incompressible, simulations carried out in OpenFOAM. The airfoil chord c is set at 132 mm, and the cylinder diameter D is fixed at 25 mm. Three streamwise spacings—2D, 6D, and 10D—are taken into account. Lift coefficient, Drag coefficient, turbulence intensity fields, and velocity fields plots can be useful for better understanding the phenomena. These results can be helpful in calculating the Strouhal number. This case tries to understand and simulate the ways in which wake structures impact and affect the downstream airfoil's aerodynamics by comparing these quantities across the three spacing configurations.

In order to capture unsteady fluid–structure interaction, the project proposal initially called for simulating a pitching airfoil using dynamic mesh and thus using pimpleDyMFoam. The necessary dynamic-mesh simulations, however, would be more computationally demanding than the available power and significantly increased the time needed to obtain the results, according to initial computational calculations. As a result, the investigation's focus was narrowed to a stationary airfoil at angles of attack of zero and five degrees. Despite removing rotational effects, this simplification maintains the main goal of measuring wake-induced unsteady loading and offers a computationally feasible framework for researching wake–body interactions. Thus, considering these computational limits, we're focusing on a limited time study with non-dynamic meshing of the airfoil.

2. Problem Statement

The objective of this case study is to quantify and study the aerodynamic interaction between the wake generated by a circular cylinder and a downstream NACA 0012 airfoil held at zero-

and five-degrees angle of attack. In practical applications such as aircraft in formation flight or wind-turbine row configurations, the wake of upstream bluff bodies can result in significant fluctuations in downstream bodies and alter the performance of downstream lifting surfaces.

In this work, a two-dimensional incompressible unsteady flow is simulated using pimpleFoam solver in OpenFOAM. The setup consists of a circular cylinder of diameter $D=25mm$ placed upstream of a NACA 0012 airfoil of chord length $c=132mm$. Three streamwise spacings between the cylinder centreline and the airfoil leading edge are considered:

- ***2D*** *(50 mm)*
- ***6D*** *(150 mm)*
- ***10D*** *(250 mm)*

The computational domain is extruded minimally (240mm) in the spanwise direction to permit a three-dimensional mesh, while preserving two-dimensional flow physics. Thus, the new domain has dimensions 750 × 240 mm. The primary goals of the study are:

1. To visualize the velocity and turbulence intensity fields in the cylinder wake and around the airfoil for each spacing.
2. To determine the lift and drag coefficients on the airfoil, including their mean values and unsteady fluctuations, as functions of cylinder–airfoil separation.

Simulations are performed with the transient pimpleFoam solver, using mesh refinement in the wake region to resolve vortical structures and boundary layers. Results will be compared across the three cases to reveal the dependence of aerodynamic forces on the influence by upstream wake.

3. Governing Equations

The fluid flow over the cylinder-airfoil configuration is considered two-dimensional, unsteady, incompressible, and viscous [3]. Under these conditions, Reynolds-Averaged Navier–Stokes equations using the basic conservation equations of continuity and momentum are as follows

Continuity:

$$\nabla \cdot \mathrm{U} = 0 \Rightarrow \frac{\partial u_i}{\partial x_i} = 0$$

Equation 1: Continuity Equation

Momentum:

$$\frac{\partial \bar{U}}{\partial t} + (\bar{U} \cdot \nabla)\bar{U} = -\frac{1}{\rho}\nabla \bar{p} + \nu \nabla^2 \bar{U} - \nabla \cdot \overline{u'u'}$$

Equation 2: Momentum Equation

Where $\bar{U}$ and $\bar{p}$ is the time-averaged velocity and pressure, ρ is the density, ν is the kinematic viscosity, and $\overline{u'u'}$ is the Reynolds stress tensor. This term accounts for the momentum transport due to turbulent fluctuations.

These governing equations are discretized and marched in time by the PIMPLE (PISO–SIMPLE hybrid) algorithm in OpenFOAM, using second-order spatial schemes (upwind for convection, central for diffusion) and a backward-differencing temporal scheme, while ensuring a maximum Courant number below unity for numerical stability. The Shear Stress Transport (SST) model combines the benefits of the k-ω and k-ε models. It uses the k-ω model near the wall to resolve the boundary layer accurately and the k-ε model away from the wall to handle adverse pressure gradient flows. The SST model provides improved predictions for a wide range of flow conditions. Thus k–ω SST model was used for turbulence [5]. Hence two additional transport equations for turbulent kinetic energy (k) and the specific dissipation rate (ω) are used as well. The model is used since the study involves turbulent flow. The detailed equations can be understood at Menter's Shear Stress Transport Page.

4. Simulation Procedure

4.1 Geometry and Mesh

The required geometries were created in SOLIDWORKS, exported as a STEP file, and subsequently converted to an STL surface representation using Salome. The configuration comprises a circular cylinder of diameter $D=25\,mm$ and, downstream in its wake, a NACA0012 airfoil of chord length $c=132\,mm$. Three streamwise spacings between the cylinder centreline and airfoil leading edge were considered: 2D, 6D, and 10D. To satisfy OpenFOAM's requirement for a three-dimensional mesh, the 2D geometry was extruded uniformly in the spanwise (z) direction by one cell thickness. The same procedure was repeated for the airfoil at an angle of attack of 5 degrees.

The nominal computational domain was initially chosen as 35c in the streamwise (x) direction by 20c in the vertical (y) direction, as illustrated in Figure 4.1.1 which was how it was solved in the referred paper [1]. However, this large domain proved too demanding for the available computational hardware and power. After initially testing with this big domain, it was reduced to $742mm \times 160mm \times 170\ mm$ (Figure 4.1.2), which still ensured minimal boundary interference with the wake–airfoil interaction while significantly lowering cell counts. Therefore, second domain is chosen for simulations from now on, as it allows for a finer mesh and a longer simulation time.

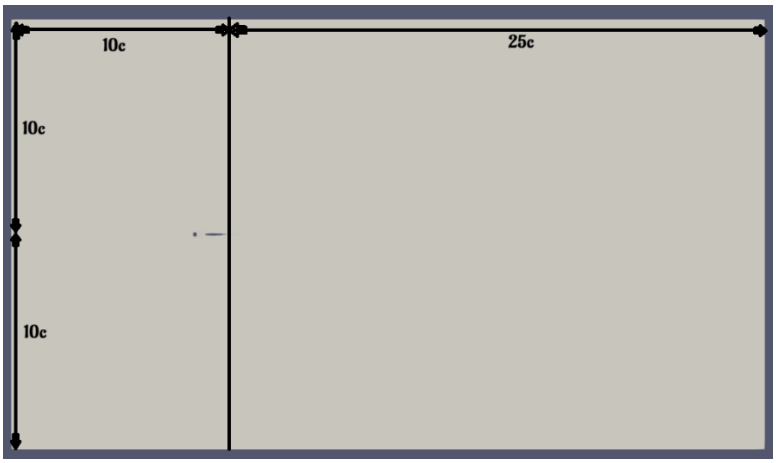

Figure 1: Initial Domain chosen in the paper

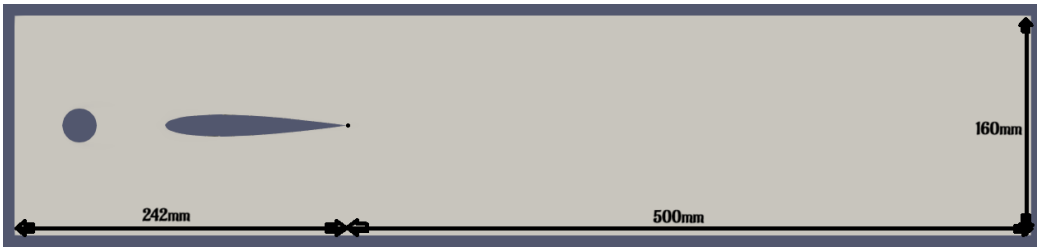

Figure 2: Modified domain for our study

Meshing was performed in two stages:

1. **blockMesh**

   A structured base mesh was defined in the blockMeshDict file, creating a single hexahedral block encompassing the entire domain. The base mesh resolution was set to 500 cells in x, 500 cells in y, and 1 cell in z, yielding an initial grid of approximately 250,000 cells.

2. **cfMesh** **Refinement**

   To capture the fine-scale wake structures and boundary layers, cfMesh was employed

for unstructured refinement. An anisotropic refinement surface was created along the domain centreline:

- A narrow box of dimension $(Lx \times Ly) = (500mm \times 60mm)$ centred on the wake region was defined to enforce high resolution. Here the cells in y-axis were squeezed by scale of 0.3.
- Mesh grading in the y-direction was squished to achieve a minimum cell height of 0.1 mm near the cylinder and airfoil surfaces, targeting y+<1.
- Away from this refinement zone, cell sizes gradually increased up to 8 mm to reduce total mesh size.

Overall, the final mesh for each spacing case contained on the order of *473,000 – 763,000* cells, with a maximum face size of 9.29×10^{-5} mm^2 and aspect ratio of 25. The mesh is unstructured but delivers proper results. Figure 4.1.3 shows the combined blockMesh + cfMesh grid around the cylinder–airfoil assembly for gap of 2D. Mesh quality checks (cell aspect ratio, non-orthogonality, skewness) confirmed that the grid meets best practices for transient incompressible flow simulations. The mesh could not be further refined because of limited computational facilities and limitations.

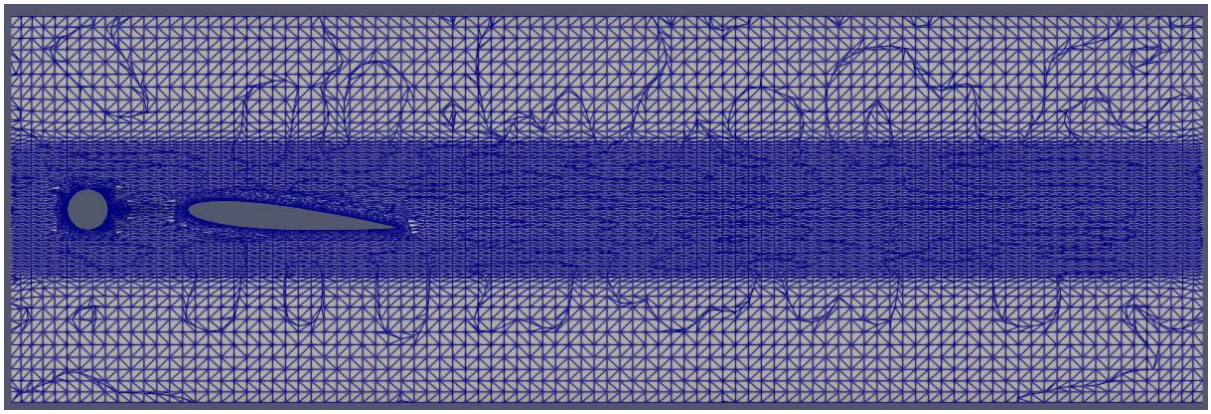

Figure 3: Computational mesh around the cylinder-pitching airfoil configuration

The mesh was validated for proper results by simulating only the airfoil, with same inlet velocity and the resulting lift and drag coefficients matched the already derived results.

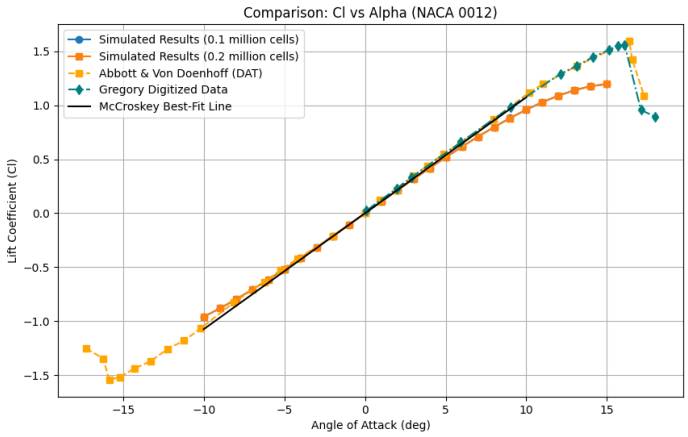

Figure 4: Validation of NACA0012 airfoil

4.2 Initial and Boundary Conditions

All cases in this study were conducted at a free-stream velocity of $U_\infty = 11.06m/s$ corresponding to Reynolds number of $Re = (U_\infty c)/\nu = 100000$ based on the airfoil chord(c) and another based on the cylinder, $Re(D) = 19250$.

U_{inlet}	11.06m/s
p_{outlet}	0 Pa
Angle of Attack(degrees)	0,5
Cylinder and Airfoil Walls	No-Slip
Top and Bottom Faces	Walls

4.3 Solver

The transient, incompressible flow simulations were carried out using OpenFOAM's pimpleFoam solver. This solver implements the PIMPLE algorithm, which combines the PISO (Pressure Implicit with Splitting of Operators) approach for transient pressure–velocity coupling with the SIMPLE (Semi-Implicit Method for Pressure-Linked Equations) corrections to enhance stability at larger time steps. Although the details are handled internally, pimpleFoam is well suited for unsteady turbulent flows because it can maintain a Courant number below unity while efficiently marching in time. Spatial discretization was performed with second-order upwind schemes for convective terms and central differencing for diffusion. Time integration uses a second-order backward-differencing method. Since the Reynolds numbers considered in this study fall within the turbulent regime, a RANS turbulence model

was employed. The k–ω SST model was used to close the Reynolds-Averaged Navier–Stokes equations, allowing for the prediction of turbulent transport in the boundary layers and wake regions. These settings provide a good balance between accuracy and time for arriving for the final results. Although the timestep chosen was very small, but the solver was quick in its ways to arrive at the solution.

5. Results and Discussions

The present study involves six simulation cases corresponding to combinations of three streamwise spacings (2D, 6D, and 10D) and two angles of attack (0° and 5°). Based on the computational resources available, each case was simulated up to a dimensional physical time of 0.2 seconds. Important information was extracted from the flow fields, probe signals, and aerodynamic force plots and graphs despite this comparatively brief simulation window.

Karman vortex street was not seen within the allotted simulation time, despite the employment of a RANS-based turbulence model (k–ω SST). This is probably because the wake didn't have much time to develop. Thus, there were no clear periodic vortex shedding structures in vorticity fields. However, enough information is available to analyze wake behaviour and downstream airfoil interaction thanks to probe-based velocity time series, instantaneous velocity contours, and turbulence intensity fields. A more accurate representation of vortex generation could be achieved through the use of advanced turbulence modelling approaches, such as Large Eddy Simulation (LES) or Detached Eddy Simulation (DES) or Direct Numerical Simulation (DNS). The following are the velocity contours (unit is m/s) for the cases with varying gaps:

1. Angle of Attack: 0°

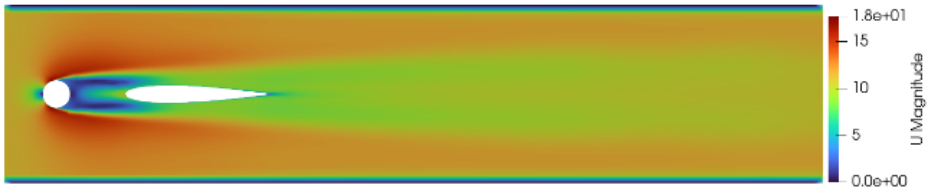

Figure 5: Gap 2D

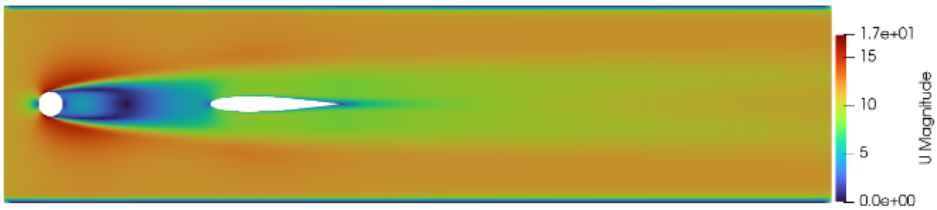

Figure 6: Gap 6D

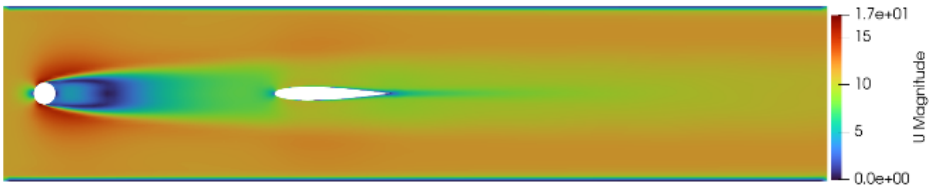

Figure 7: Gap 10D

2. Angle of Attack: 5°

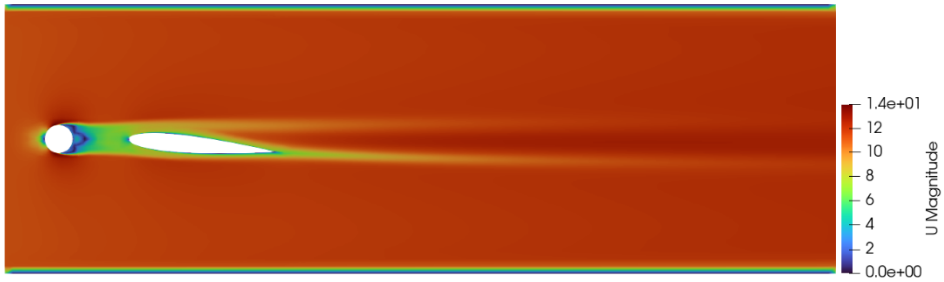

Figure 8: Gap 2D

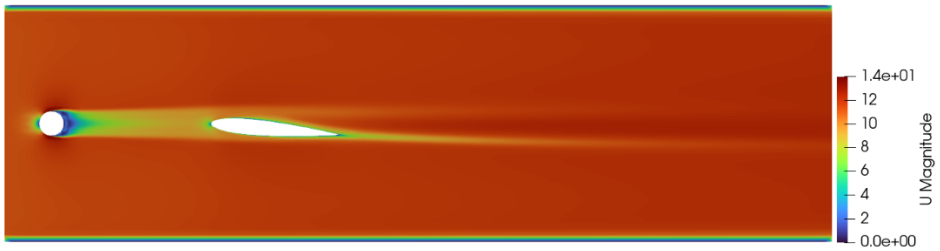

Figure 9: Gap 6D

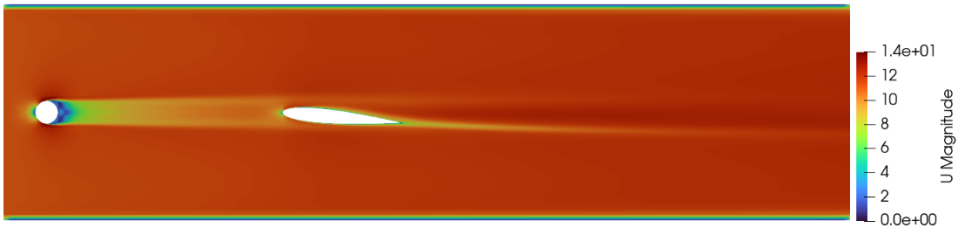

Figure 10: Gap 10D

The instantaneous velocity magnitude contours for each of the six configurations are shown in Figures 5 through 10. The flow field downstream of the cylinder exhibits a comparatively smooth transition as the spacing increases in the 0° AoA cases. The wake directly impacts the airfoil for 2D spacing, changing the boundary layer and pressure distribution on both surfaces. A more uniform flow results from the wake dissipating and its impact on the airfoil diminishing as spacing increases to 6D and 10D.

Because of the geometric inclination, the flow field downstream of the airfoil is asymmetric in the 5° AoA cases. Particularly at smaller spacing (2D), the slight deflection causes areas of mild separation and lower velocity in the near-wake region, which are made worse by upstream disturbances from the cylinder. The following are the turbulent intensity contours (unitless) for the cases with varying gaps:

1. Angle of Attack 0°

Figure 11: Gap 2D

Figure 12: Gap 6D

Figure 13: Gap 10D

2. Angle of Attack 5°

Figure 14: Gap 2D

Figure 15: Gap 6D

Figure 16: Gap 10D

For every case, the turbulence intensity (TI) plots in Figures 11 through 16 demonstrate high turbulence levels in the cylinder's wake. Turbulence spreads across both surfaces in the 2D configuration because the wake keeps its energy and interacts directly with the airfoil. The TI decays before it reaches the airfoil at larger spacings (6D and 10D), suggesting partial wake recovery. Because of flow asymmetry and increased shear from inclination, the TI values in the 5° AoA cases exhibit slight amplification close to the trailing edge.

The velocity time histories from these probes (Figure 17) show how the flow evolves in space and time. For 0° AoA, velocity fluctuations were more prominent in the 2D case, gradually stabilizing at 6D and 10D. The 5° AoA cases exhibited consistent upstream signals but slightly altered downstream behaviour due to mild asymmetry in the flow path.

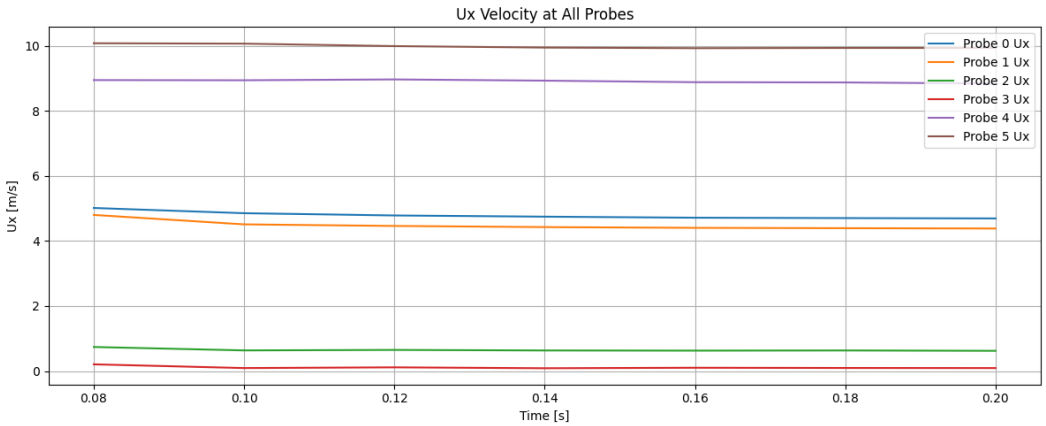

Figure 17: Velocity graphs of the probes with time

The Uy (transverse) component from Probe 0 was used to extract the dominant frequency via Fast Fourier Transform (FFT), which was then used to compute the Strouhal number. Other than Probe 0, any other can be used to reach the same result, which was verified with the help of the code written in Python used to calculate and derive the plots and calculations provided below and in Fig 17.

As observed, the velocity measured by the probes converges to a steady value after a certain period. These velocity signals are instrumental in determining other flow parameters. By plotting the velocity time series at each probe and performing Fast Fourier Transforms (FFTs), the vortex shedding frequency can be extracted. This frequency is then used to calculate the Strouhal number, which directly quantifies the vortex shedding characteristics.

The FFT converts time-domain signals into their frequency-domain representations. For an oscillating velocity signal $u(t)$, the FFT reveals the dominant frequencies and their amplitudes. In unsteady flows, transverse velocity fluctuations occur near the wake region, for example, the U_y component measured at a probe. By applying FFT to signals such as $U_y(t)$ or the lift coefficient $C_l(t)$, the dominant frequency corresponding to vortex shedding can be identified.

The Strouhal number is a dimensionless parameter that characterizes the vortex shedding frequency relative to the flow velocity and characteristic length of the body. It is mathematically defined as:

$$St = \frac{fU_\infty}{D}$$

Equation 3: Strouhal Number

Here, f represents the vortex shedding frequency obtained from the FFT analysis, D is the characteristic length (cylinder diameter), and U_∞ denotes the free-stream velocity. Based on the Strouhal number graphs, it can be inferred that the Strouhal number St is approximately 0.2 when D is taken as the cylinder diameter.

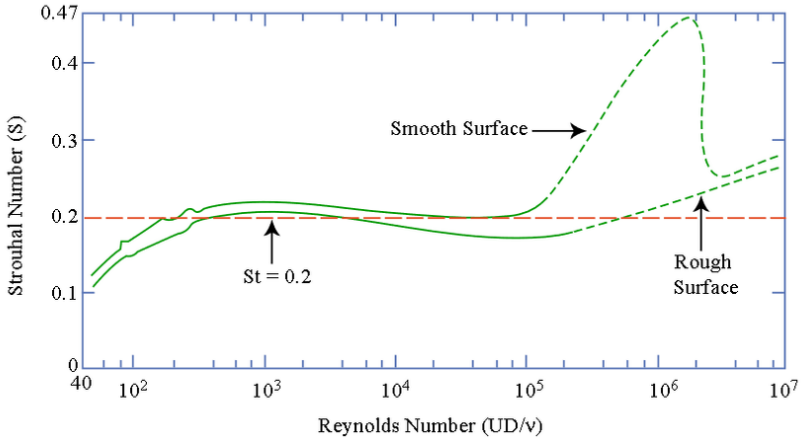

Figure 18: Strouhal number with varying Reynolds number

We now proceed to examine the results obtained from the simulated cases. Although a comprehensive set of graphs is available in the accompanying folder for reference, only the values will be presented here for clarity.

Gap	$AoA(°)$	$f(Hz)$	St	$mean(C_l)$	$mean(C_d)$	ΔC_l	ΔC_d
2D	0	20.0020	0.2387	0.0933	0.0934	0.0008	0.0007
6D	0	14.2856	0.1705	0.1010	0.1010	0.0015	0.0015
10D	0	14.2851	0.1705	0.1032	0.1031	0.0036	0.0038
2D	5	5.8828	0.0702	0.0088	0.0088	0.0083	0.0083
6D	5	14.9996	0.1790	0.0091	0.0091	0.0070	0.0070
10D	5	40.0000	0.4774	0.0093	0.0093	0.0000	0.0000

Table 1: Results from the Probes

The Strouhal numbers for 0° AoA align well with the expected range (St of approx. 0.2), especially for 2D spacing. For the 5° cases, however, the vortex shedding behaviour appears more irregular. The 2D and 10D configurations deviate significantly from expected Strouhal values, indicating interference effects and instability in vortex formation at inclined angles. Notably, the 10D–5° case shows an unusually high frequency and zero fluctuation in aerodynamic forces, suggesting numerical problems in calculations or incomplete development due to short simulation time which is more probable. The mean C_l and C_d are very close to zero but not exactly because of the wake moving downstream and its effects.

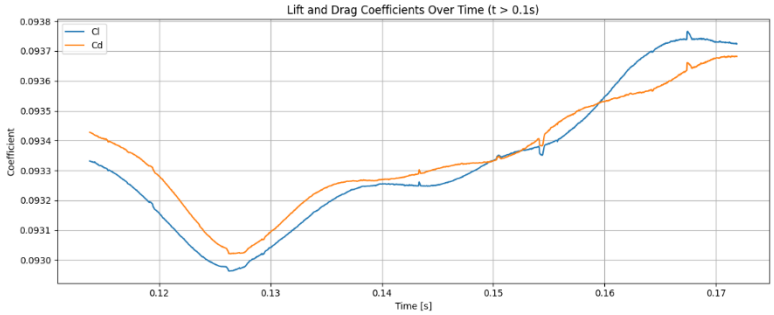

Figure 19: Cl and Cd plot for 2D case

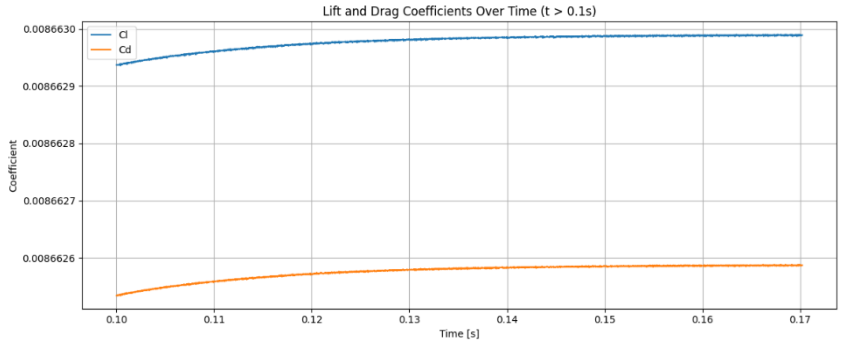

Figure 20: Cl and Cd plot for 2D inclined case

For the case where only airfoil was simulated, we had derived the standard results of lift coefficient of 0 and drag coefficient of 0.006 was found. And for airfoil inclined at 5 degrees, the coefficients were 0.56 and 0.001. Thus, we can see because of the cylinder, there are variations in the lift and drag coefficients. We can see the direct relationship that increasing the gap, increased the mean lift and drag coefficient. This implies that greater the separation, more the flow improves reattachment and recovery of pressure by allowing the airfoil to avoid the wake's damaging effects. But for the same gap, if the angle of attack was changed from zero to five, there is a reduction in these values. Hence, the gap and the angle of attack determine the changes in the lift and drag coefficients in the particular setup. Not according to the expectations, the mean values for the 5° AoA cases are lower. This could be explained by the inclination changing the direction and area of effective flow, which lowers net aerodynamic forces and direct wake impingement. This behaviour emphasizes how intricate wake-airfoil interactions are and how important spatial alignment is.

Thus, if we summarize the whole case study project, then there are a few points which we can understand. The strongest wake–airfoil interaction is observed in the 2D spacing cases, with higher turbulence levels and larger force fluctuations. If the space between the cylinder and airfoil is increased (6D and 10D), the aerodynamic behaviour is more stable, and the wake

dissipation. The velocity difference between the wake and the free-stream diminishes as the distance from the airfoil increases, while the wake width expands. This behaviour can be because of the influence of the no-slip condition at the airfoil surface on the downstream flow with increasing distance from the airfoil [2]. The 0° AoA cases show expected vortex shedding frequencies and their Strouhal numbers. At 5° AoA, the wake goes irregular and with lower shedding frequencies (except the 10D case) and reduced lift and drag mean coefficients. The Force fluctuations (ΔCl *and* ΔCd) were nearly zero for all the cases but more prominent at closer gaps, thus we can observe the shielding effect of spacing. Also, we couldn't clearly visualize the vortex formations and had some anomalous frequency (10D, 5° AoA), suggesting to have a longer simulation time for future studies.

Figure 21: Velocity Contour

Figure 22: Turbulent Intensity Contour

As for to check out the missing vortices in the plots, a single cylinder geometry was developed and then under the same conditions simulated as well. The goal was to verify if the characteristic Karman vortex street would emerge under the same meshing and solver conditions. The simulation was carried out using the same turbulence model (k−ω SST), with

a little coarser mesh (717,000), and a freestream velocity of 11.06 m/s. Despite extending the simulation up to 1.0 s, the results did not show any clear vortex street formation or unsteady oscillations in the aerodynamic forces. The lift and drag coefficients remained nearly constant throughout the simulation, with peak-to-peak fluctuations below 0.0001. Similarly, the computed Strouhal number based on the transverse velocity at a probe behind the cylinder was only 0.0149, significantly lower than the expected range of 0.18–0.22 for a circular cylinder at comparable Reynolds numbers. While these results do not match or come up even close from the classic cylinder wake behaviour reported in literature, they do not indicate incorrect physics but rather, they reflect the computational limitations by such a small time and region with not a fine mesh and the selected model. The overall trends in force behaviour across the main cases, such as increased force fluctuations at closer spacing, still support the qualitative understanding of wake–airfoil interactions.

References

[1] Rad, M. P., & Khoshnevis, A. B. (2025). Experimental and numerical study of a pitching airfoil interacting with the vortical wake of an upstream cylinder. *Ocean Engineering*, *322*, 120559. https://doi.org/10.1016/j.oceaneng.2025.120559

[2] Rad, M. P., & Khoshnevis, A. B. (2023). Experimental investigation of flow structure over pitching airfoil in the wake of circular cylinder. *Ocean Engineering*, *284*, 115103. https://doi.org/10.1016/j.oceaneng.2023.115103

[3] Cengel, Y. A., & Cimbala, J. M. (2004). *Fluid Mechanics: Fundamentals and Applications*. http://ci.nii.ac.jp/ncid/BB04830554

[4] Patankar, S. V. (2018). Numerical heat transfer and fluid flow. In *CRC Press eBooks*. https://doi.org/10.1201/9781482234213

[5] Trieu, T. C. Two-Equation Eddy-Viscosity Turbulence Models for Engineering Applications. https://doi.org/10.2514/3.12149